


## Absolute cross sections and asymmetry parameters for the photodetachment and binding energy of excited $C^-(^2D^o)$

Raphaël Marion<sup>\*,†</sup> and Xavier Urbain<sup>‡</sup>

*Institute of Condensed Matter and Nanosciences, Université Catholique de Louvain, Louvain-la-Neuve B-1348, Belgium*

 (Received 17 September 2023; accepted 7 December 2023; published 26 December 2023)

This paper presents experimental results for the photodetachment of the excited state ( $^2D^o$ ) of the carbon anion. The animated crossed beam technique is used to measure the absolute cross section for photodetachment with photon energies ranging from 0.12 to 2.7 eV, shedding light on a long-standing discrepancy between existing theoretical approaches. A velocity map imaging spectrometer is used to determine partial cross sections and asymmetry parameters. An update of the binding energy of  $C^-(^2D^o)$  is provided with a much improved accuracy,  $^eA_{2D^o} = 36.87(3)$  meV.

DOI: [10.1103/PhysRevA.108.063110](https://doi.org/10.1103/PhysRevA.108.063110)

### I. INTRODUCTION

Negative ions have been studied both theoretically and experimentally for more than a century, and have been the subject of numerous review papers [1]. Nevertheless, there are still too few experimental data, and there is often significant discrepancies with theoretical predictions.

Amongst the anions,  $C^-$  has the interesting particularity of being the lightest to possess more than one bound state (Fig. 1): the ground level,  $1s^22s^22p^3\ ^4S^o$ , and two excited levels,  $1s^22s^22p^3\ ^2D^o_{3/2}$  and  $^2D^o_{5/2}$ . The challenge of producing a beam with a significant population of excited states makes it difficult to characterize them, explaining why experiments devoted to the precise determination of electron affinity  $^eA$  [2,3] produce results for the ground state only.

Photodetachment of the  $^2D^o$  state is poorly known. In the near-infrared and visible range, it involves two distinct final states, as depicted in Fig. 1, that coexist with the photodetachment of the  $^4S^o$  ground state:

$$C^-(^4S^o) + \gamma \longrightarrow C(^3P) + e^-(s, d; \varepsilon_1), \quad (1)$$

$$C^-(^2D^o) + \gamma \longrightarrow C(^3P) + e^-(s, d, g; \varepsilon_2), \quad (2)$$

$$C^-(^2D^o) + \gamma \longrightarrow C(^1D) + e^-(s, d, g; \varepsilon_3), \quad (3)$$

with  $\varepsilon_i$  the kinetic energy of the ejected electron.

Partial and total cross sections have only been measured for  $E_{\text{ph}} = 2.076$  eV [4]. That work followed an experimental study [5], led at same energy, of the asymmetry parameter  $\beta$  that characterizes the differential cross section:

$$\frac{d\sigma_i}{d\Omega} = \frac{\sigma_i}{4\pi} [1 + \beta_i P_2(\cos\theta)]. \quad (4)$$

Finally, two theoretical calculations based on the  $R$ -matrix approach have been elaborated [6,7], with predictions around

thresholds presenting strong disparities. These significant departures illustrate the acute sensitivity to electron correlations specific to anionic systems and show the necessity of highly accurate experimental data for benchmarking state-of-the-art theoretical methods and refining the description of fundamental negative ions such as  $C^-$ .

This paper reports the total and partial cross sections and asymmetry parameters obtained for photon energies ranging from 0.12 to 2.7 eV (corresponding to wavelengths between 10.6  $\mu\text{m}$  and 457 nm) where the disagreement between existing calculations is particularly pronounced. Absolute experimental cross sections have been obtained over the whole range while proper differential cross sections in the same range have also been measured. Moreover, our results provide an improved value of the binding energy  $^eA$  of the excited state of  $C^-$  with an uncertainty reduced by more than an order of magnitude.

The structure of the paper is as follows: the experimental setup and data analysis methods are described in Sec. II, results are detailed and discussed in Sec. III, and conclusions and perspectives are presented in Sec. IV.

### II. EXPERIMENTAL SETUP

Following the ideas developed in [8], we produce an anion beam with a high proportion of excited states by charge exchange between a beam of  $C^+$  and Cs vapor. In our experimental setup, depicted in Fig. 2, the positive beam is produced by a duoplasmatron source filled with  $\text{CO}_2$  gas, with an energy of 5 keV. A permanent magnet performs a mass selection, the  $C^+$  ions being directed through a 5-cm-long Cs vapor cell operated at a temperature of 390 K. The electrostatically separated and collimated  $C^-$  beam (diameter 1 mm, current 50 pA) is eventually chopped by an electrostatic deflector in front of an aperture to limit detector aging during pulsed measurements. The beam then interacts with a laser in a crossed beam geometry.

In order to cover the entire wavelength range from 457 nm to 10.6  $\mu\text{m}$ , we use a wide set of laser light sources. The pulsed light source is an OPO laser system (NT342A-30,

\*raphael.marion@uclouvain.be

†Present address: Royal Observatory of Belgium, Avenue Circulaire 3, B-1180 Brussels, Belgium.

‡xavier.urbain@uclouvain.be

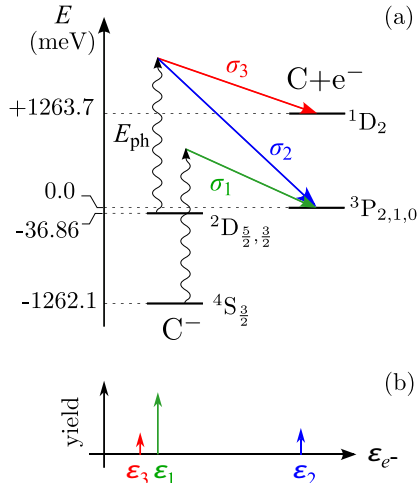


FIG. 1. (a) Energy levels with proposed  $A$  value for the  $2D^{\circ}$  state. (b) Typical photodetached electron spectrum. The relative yields depend on initial populations and cross sections which vary with photon energy  $E_{\text{ph}}$  (see Fig. 4 for more details).

Ekspla), tunable from 2600 to 225 nm, with a repetition rate of 30 Hz. Pulse energies are kept below  $20 \mu\text{J}$  to limit the saturation of the photodetachment. Continuous light sources, with power ranging from 100 mW to 5 W, are provided by different solid-state lasers at 457, 532, 1064, and 1550 nm; a  $\text{CO}_2$  laser at  $10.6 \mu\text{m}$ ; and, for the part of the spectrum overlapping with the respective photodetachment thresholds of the  $\text{C}^-$  ( $4S^{\circ}$ ) to  $\text{C}(^3P)$  and  $\text{C}^-$  ( $2D^{\circ}$ ) to  $\text{C}(^1D)$  transitions, by a tunable Ti-sapphire laser ranging from 700 to 1000 nm (3900S from Spectra-Physics). All laser beams are collimated to a spot size similar to the anion beam diameter.

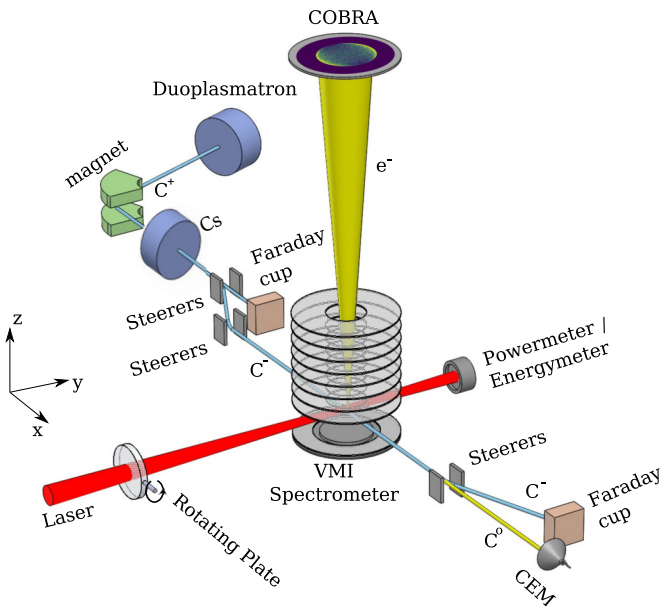


FIG. 2. Experimental setup. The laser beam is swept vertically by tilting a thick glass plate. COBRA is a detection system correlating the brightness of the light spots with the amplitude of the electrical signals [9].

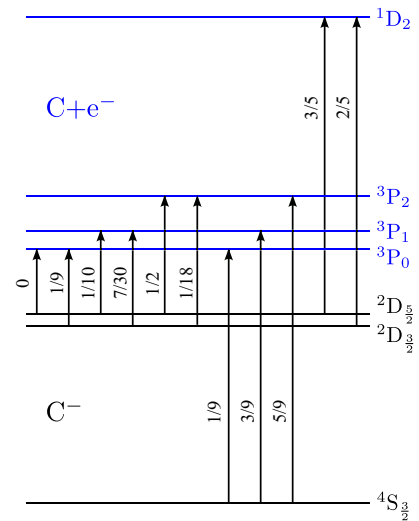


FIG. 3. Theoretical fine-structure-resolved relative intensities for the photodetachment of  $\text{C}^-$ . Level spacing and position are not to scale.

Detailed information on our detection techniques can be found in previous papers [10–12]. We thus summarize their main features hereafter in Secs. II A and II B.

### A. Velocity map imaging

Angle- and energy-resolved photoelectron spectroscopy gives access to partial and differential cross sections, as well as the electron binding energy. Our velocity map imaging (VMI) spectrometer is based on the position-sensitive detection of photoelectrons, extracted perpendicularly to the laser and anion beams by an electrostatic lens. Photoelectrons are detected using a detection system correlating the brightness of the light spots with the amplitude of the electrical signals (COBRA) [9]. It consists of three stacked microchannel plates, a phosphor screen, a CMOS camera, and a waveform digitizer. This detector is placed at the focal plane of an electrostatic lens and is parallel to the polarization axis of the laser light.

The spatial distribution of hits corresponds to the Abel projection, onto the plane of the detector, of a superposition of several Newton spheres, as depicted in the left-hand part of Fig. 4(a). To disentangle the radial two-dimensional (2D) distribution and retrieve the one existing in three dimensions (3D) before the projection (solving the so-called Abel inverse problem), a homemade routine based on Bayesian analysis of the radial distribution has been developed [13] to extract the radius  $r_i$  together with the number of events  $A_i$  associated to each channel, even when not all channels are clearly resolved.

The radius of a Newton sphere  $r_i$  is proportional to the electron velocity times the time of flight through the spectrometer. As the electron energy  $\varepsilon_i$  is proportional to the total kinetic energy  $K_i$  of the fragments, under conservation of energy and momentum with the recoiling atom,

$$K_i = \left(1 + \frac{m_e}{M_C}\right) \varepsilon_i, \quad (5)$$

the radius  $r_i$  is proportional to the square root of the total kinetic energy  $K_i$  with a common calibration parameter  $\alpha$

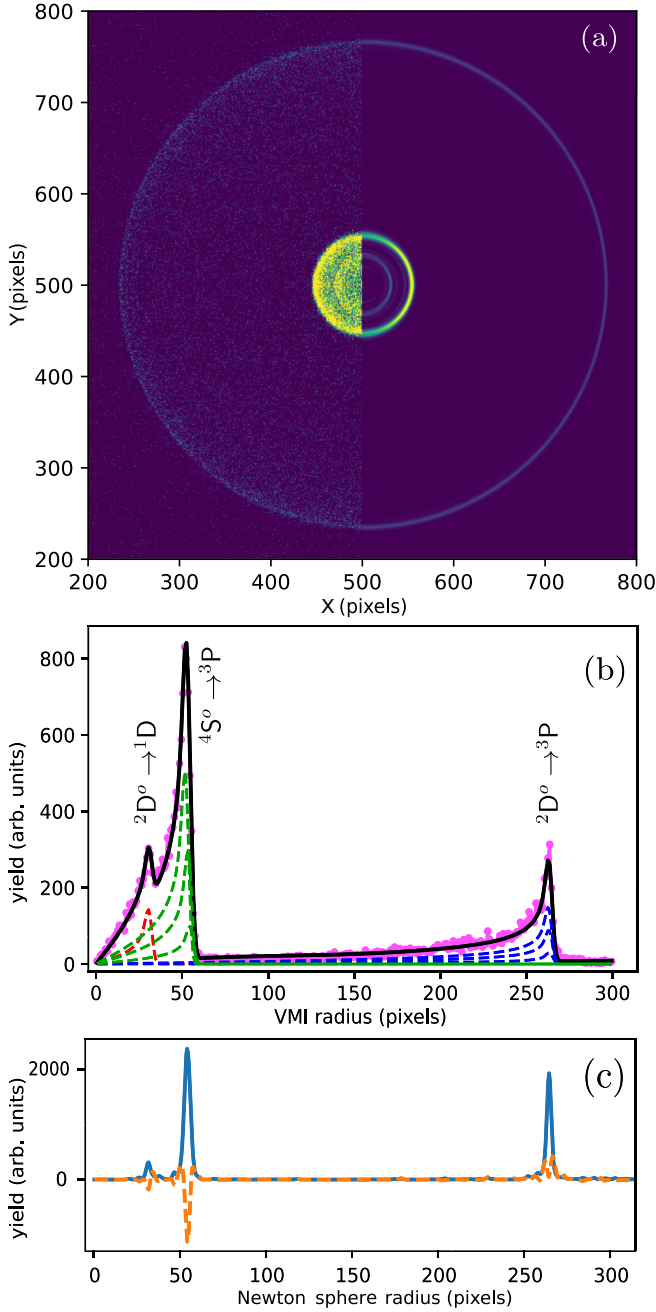


FIG. 4. (a) Left: 2D histogram of experimental distribution recorded at  $\lambda = 940$  nm. Right: Azimuthal section of the 3D reconstruction of Newton spheres. (b) The dotted line is the radial distribution of experimental events. Dashed lines are the Bayesian estimation of each channel, colors code following Fig. 1, while the solid line is the cumulative reconstruction. (c) MEVELER spectrum giving  $q_0$  (solid line) and  $q_2$  (dashed line).

accounting for the properties of the VMI lens and the mass factor introduced above:

$$r_i = \alpha \sqrt{K_i}. \quad (6)$$

$K_i$  is equal to the photon energy  $E_{\text{ph}}$  minus the detachment energy, which is the difference between the energy level of

the residual atom and that of the initial state. Adding the fine-structure label  $J$  of the residual atom, we have

$$\begin{aligned} K_{1J} &= E_{\text{ph}} - (E_{3P_J} - E_{4S^0}) \\ &= E_{\text{ph}} - (E_{3P_J} - E_{3P_0}) - \epsilon A_{4S^0}, \end{aligned} \quad (7)$$

$$\begin{aligned} K_{2J} &= E_{\text{ph}} - (E_{3P_J} - E_{2D^0}) \\ &= E_{\text{ph}} - (E_{3P_J} - E_{3P_0}) - \epsilon A_{2D^0}, \end{aligned} \quad (8)$$

$$\begin{aligned} K_{32} &= E_{\text{ph}} - (E_{1D_2} - E_{2D^0}) \\ &= E_{\text{ph}} - (E_{1D_2} - E_{3P_0}) - \epsilon A_{2D^0}. \end{aligned} \quad (9)$$

For initial and final states exhibiting fine structure, photodetachment occurs between various initial and final fine-structure components [11,14,15] which slightly broadens the distribution of total  $A_i$  events and hence the uncertainty in the evaluation of the point-spread function of the spectrometer.

This distribution reflects the relative intensities of the threshold photodetachment of a  $p$  electron, which take the general form [15–17]

$$\begin{aligned} I_{J'J} &= [J'] [J] \sum_{\lambda} [\lambda] \left\{ \begin{matrix} L & S' & \lambda \\ \frac{1}{2} & J & S \end{matrix} \right\}^2 \\ &\times \left\{ \begin{matrix} L & S' & \lambda \\ J' & 1 & L' \end{matrix} \right\}^2, \end{aligned} \quad (10)$$

with the abbreviated notation  $[J] = 2J + 1$ . The quantum numbers  $(L', S', J')$  and  $(L, S, J)$  are relative to the anion and the atom respectively. The relative intensities are normalized such that  $\sum_{J', J} I_{J'J} = 1$ , as a result of the symmetry and orthogonality properties of  $6j$  symbols [18]. The intensity distribution given by Eq. (10) is still valid far from threshold if the one-electron dipole matrix elements are term independent, as theoretically discussed by Pan and Starace [16] and experimentally verified for the  $O^-$  anion by Cavanagh *et al.* [19].

Direct evaluation of Eq. (10) produces the relative intensities given in Fig. 3. A population of the  $3P_J$  levels of the neutral atom in proportion of their multiplicities is thus expected sufficiently far above threshold in the case of the  $4S^0$  initial state of the negative ion. For the  $2D^0$  initial state, however, the values of the final-state populations depend on the population of the initial-state fine-structure components.

A reasonable assumption in the present experiment is that  $2D_{3/2}^0$  and  $2D_{5/2}^0$  are populated in proportion of their multiplicities due to the minute fine-structure splitting between them [20] and the energetic collisions in which they are created. Under these conditions, the relative intensities computed above also produce a population of the  $3P_J$  levels in proportion of their multiplicities. The total number of events  $A_i$  associated to a given  $L_i S_i$  term is thus distributed among its fine-structure components according to

$$A_{iJ_i} = \sum_{J'} I_{J', J_i} A_i = \frac{[J_i]}{[L_i][S_i]} A_i. \quad (11)$$

Very close to threshold, this distribution deviates from Eq. (10) and may be modeled by introducing cross sections following the Wigner threshold law for  $s$ -wave scattering. This more involved fitting procedure is however not

needed here since the energy resolution of the spectrometer increases close to threshold as it operates on a velocity scale, allowing for a direct fit of individual fine-structure components.

Henceforth, including the Gaussian point-spread function of the spectrometer, parametrized by a standard deviation  $\delta$  identical for all channels, as well as a uniform background  $b$ , the set of parameters to be estimated is then  $X = \{A_i\}_{i \in \{1,2,3\}}, A_{2D^0}, E_{\text{ph}}, b, \alpha, \delta\}$ . We consider broad priors for each of them, except for  $E_{\text{ph}}$  which is known with better precision. A typical reconstruction is presented in Fig. 4(b).

It should be noted that the calibration parameter  $\alpha$  is internally constrained to a much higher level than our determination of the photon energy, and that

$$\begin{aligned} E_{3p_0} &= 0.000\,00(16) \text{ meV}, \\ E_{3p_1} &= 2.035\,41(16) \text{ meV}, \\ E_{3p_2} &= 5.382\,56(16) \text{ meV}, \end{aligned} \quad (12)$$

$$E_{D_2} = 1263.7284(4) \text{ meV}, \quad (13)$$

$$A_{4S^0} = 1262.1226(11) \text{ meV} \quad (14)$$

may be considered as constants as they are known [3,21] with uncertainties far smaller than our experimental ones (digits in parentheses are the uncertainty, to the precision of the same number of least significant digits).

The asymmetry parameters  $\beta$  are obtained by means of the MEVELER algorithm [22] based on free-form reconstruction. In this algorithm, hypothetical Newton spheres are associated to all possible values of radial velocity and the corresponding amplitudes are optimized to reproduce the data under the constraint of maximization of the entropy of the priors (MaxENT). This approach, which works very well for sufficiently separated electron energies, defines the angular distribution of events for a given velocity  $v$ , related to the differential cross section (4), as

$$\mathcal{P}(v, \theta, \phi) = \frac{1}{4\pi v^2} [q_0(v) + q_2(v)P_2(\cos \theta)]. \quad (15)$$

The evaluation of the asymmetry parameter of a particular hypothetical Newton sphere is directly given by

$$\beta(v) = \frac{q_2(v)}{q_0(v)}. \quad (16)$$

However, in order to relate these values to a physical channel, a specific velocity range must be unambiguously attributed to that channel. We have shown [12] that the quantity

$$\hat{\beta}_\ell = \frac{2\ell + 1}{N} \sum_{i=1}^N P_\ell(\cos \theta_i), \quad (17)$$

where  $N$  is the total number of events in a given channel, has all the required properties to be considered as a *good statistical estimator* of the asymmetry parameter of degree  $\ell$ . Applied to photodetachment, where the only asymmetry comes from  $\ell = 2$ , and using formula (15), it is straightforward to establish that the correct way to combine values of the different hypothetical Newton spheres, in order to obtain

a unique physical quantity, is as follows:

$$\hat{\beta} = \frac{1}{N} \int q_2(v)dv = \frac{\int q_2(v)dv}{\int q_0(v)dv}. \quad (18)$$

The integration range is limited for each channel to the interval where  $q_0(v)$  is a significant property assumed to be met for values greater than 10% of the maximum of the corresponding peak.

The great added value of using orthogonal estimators  $\hat{\beta}_\ell$  is the ability to evaluate a statistical uncertainty. For the particular case of  $\ell = 2$ , the variance simplifies [12] to

$$\text{Var}(\hat{\beta}) = \frac{5}{N} + \frac{10\hat{\beta}}{7N} - \frac{\hat{\beta}^2}{N}. \quad (19)$$

An additional difficulty arises in the present paper as the beam is not made up of a pure state but instead is a mixture of the  $4S^0$  and  $2D^0$  states. As a result, the assignment of detected events to the various channels requires the determination of two distinct quantities. The first one is the usual branching ratio between channels starting from the same state, related to the partial cross sections. With the notations of Fig. 1, we have

$$\Gamma_2 = \frac{\sigma_{2D^0 \rightarrow 3P}}{\sigma_{2D^0}} = \frac{\sigma_2}{\sigma_2 + \sigma_3} = \frac{N_{2D^0 \rightarrow 3P}}{N_{2D^0}} = \frac{N_2}{N_2 + N_3}, \quad (20)$$

$$\Gamma_3 = \frac{\sigma_{2D^0 \rightarrow 1D}}{\sigma_{2D^0}} = \frac{\sigma_3}{\sigma_2 + \sigma_3} = \frac{N_{2D^0 \rightarrow 1D}}{N_{2D^0}} = \frac{N_3}{N_2 + N_3}. \quad (21)$$

The second quantity is the ratio between the numbers of events  $N_i$  associated to each initial state:

$$\gamma_{4S^0} = \frac{N_{4S^0}}{N_{4S^0} + N_{2D^0}} = \frac{N_1}{N_1 + N_2 + N_3}, \quad (22)$$

$$\gamma_{2D^0} = \frac{N_{2D^0}}{N_{4S^0} + N_{2D^0}} = \frac{N_2 + N_3}{N_1 + N_2 + N_3}. \quad (23)$$

The number of events  $N_i$  is proportional to the corresponding partial cross section and relative population of the initial state. Assuming a uniform density of states inside the beam, we define the latter as the ratio of the current of anions in a specific state to the total current:

$$p_{4S^0} = \frac{I_{4S^0}}{I_{\text{tot}}} = \frac{I_{4S^0}}{I_{4S^0} + I_{2D^0}}, \quad (24)$$

$$p_{2D^0} = \frac{I_{2D^0}}{I_{\text{tot}}} = \frac{I_{2D^0}}{I_{4S^0} + I_{2D^0}}. \quad (25)$$

The relative contributions of the various initial states, assuming unsaturated interactions to preserve the linearity of the number of events with the cross sections, may thus be expressed as

$$\gamma_{4S^0} = \frac{\sigma_{4S^0} p_{4S^0}}{\sigma_{4S^0} p_{4S^0} + \sigma_{2D^0} p_{2D^0}} = \frac{\sigma_1 p_{4S^0}}{\sigma_1 p_{4S^0} + (\sigma_2 + \sigma_3) p_{2D^0}}, \quad (26)$$

$$\gamma_{2D^0} = \frac{\sigma_{2D^0} p_{2D^0}}{\sigma_{4S^0} p_{4S^0} + \sigma_{2D^0} p_{2D^0}} = \frac{(\sigma_2 + \sigma_3) p_{2D^0}}{\sigma_1 p_{4S^0} + (\sigma_2 + \sigma_3) p_{2D^0}}. \quad (27)$$

## B. Animated crossed beams

The animated crossed beams (ACB) technique, consisting of periodically sweeping the laser beam across the anion beam profile, provides a reliable means of accurately measuring

cross sections in an *absolute* way [10–12]. It requires that the product of the cross section  $\sigma$ , the laser intensity  $\phi_L$ , and the interaction time  $\tau$  is sufficiently small that the photodetachment process occurs within the linear regime. In the interaction zone, the anion and photon beams cross at right angles. The resulting neutrals follow a straight line trajectory and are counted with a channel electron multiplier (CEM, KBL 25RS from Sjuts Optotechnik) with a high detection efficiency, evaluated here at 93(2)%. The anion beam is deflected by electrostatic steerers to a Faraday cup measuring its current. By summing the neutral yields recorded for all possible relative vertical positions  $Z$  between the laser and anion beams, we integrate the geometrical profiles almost independently, without any further assumptions. This integration leaves only global parameters that are easily measured, such as pulse energy  $E_{p,Z}$  or laser power  $P_Z$ , current  $I_Z/e$ , and velocity  $v$  of the  $C^-$  beam and the number of neutrals detected per pulse,  $N_{p,Z}$ , or per second,  $R_Z$ .

The cross section for pulsed or continuous laser photodetachment is extracted using the following expressions [10,12], where  $Z$  is the relative position of the beams,  $\eta$  is the efficiency of the CEM, and  $n_Z$  is the number of pulses

$$\sigma_{\text{puls}}^{\text{ACB}} = \frac{1}{\eta} \sum_Z \frac{\Delta Z}{n_Z} \sum_{p=1}^{n_Z} \frac{\hbar\omega}{E_{p,Z}} \frac{ev}{I_{p,Z}} N_{p,Z}, \quad (28)$$

$$\sigma_{\text{cont}}^{\text{ACB}} = \frac{1}{\eta} \sum_Z \Delta Z \frac{\hbar\omega}{P_Z} \frac{ev}{I_Z} R_Z. \quad (29)$$

For completeness, a small correction (typically 5%) has to be applied for pulsed-laser detachment to account for deviations from the linear regime. This correction is obtained using an iterative procedure described in [12]. As a consequence of the presence of both  $^4S^o$  and  $^2D^o$  populations in the beam, the measured cross section  $\sigma^{\text{ACB}}$  corresponds to the sum of the photodetachment cross sections weighted by the relative populations of initial states in the  $C^-$  beam. With respect to the total number of events  $N = N_{^4S^o} + N_{^2D^o}$ , it is straightforward to observe that

$$\sigma^{\text{ACB}} = \sigma_{^4S^o} p_{^4S^o} + \sigma_{^2D^o} p_{^2D^o}. \quad (30)$$

As the cross section for  $^4S^o$  is experimentally well known from our previous work [12], we can combine this expression with the ratio of state-specific contributions (26) measured by VMI to determine the population (24) as

$$p_{^4S^o} = \frac{\sigma^{\text{ACB}}}{\sigma_{^4S^o}} \gamma_{^4S^o} \quad (31)$$

We can finally extract the total cross section  $\sigma_{^2D^o}$  by applying one of the following equations, as well as the partial cross sections:

$$\sigma_{^2D^o} = \frac{\sigma^{\text{ACB}} - \sigma_{^4S^o} p_{^4S^o}}{1 - p_{^4S^o}} \quad (32)$$

$$= \frac{1 - \gamma_{^4S^o}}{1 - p_{^4S^o}} \sigma^{\text{ACB}} = \frac{\gamma_{^2D^o}}{p_{^2D^o}} \sigma^{\text{ACB}}, \quad (33)$$

$$\sigma_{^2D^o \rightarrow ^3P} = \Gamma_2 \sigma_{^2D^o}, \quad (34)$$

$$\sigma_{^2D^o \rightarrow ^1D} = \Gamma_3 \sigma_{^2D^o}. \quad (35)$$

TABLE I. Experimental binding energy  ${}^eA_{2D^o}$  extracted by the Bayesian analysis of the radial distribution.

$\lambda$ (nm)	$E_{\text{ph}}$ (eV)	${}^eA_{2D^o}$ (meV)	$\Delta {}^eA_{2D^o}$ (meV)
918.43	1.3500	36.78	0.29
935.15	1.3258	36.83	0.19
940.16	1.3188	36.81	0.17
945.05	1.3119	36.84	0.19
953.06	1.3009	36.85	0.07
	Average	36.84	0.06

### III. RESULTS AND DISCUSSIONS

#### A. Electron binding energy

To the best of our knowledge, only two experimental values have been published for the binding energy of the  $^2D^o$  state: the first one obtained by field ionization gives  ${}^eA_{2D^o} = 37(3)$  meV [23] and the second one based on threshold photodetachment gives  ${}^eA_{2D^o} = 33(1)$  meV [24]. Because of its smaller uncertainty, the latter is usually considered as the reference value, as in [25] for example, an assumption that we challenge in the present paper, as detailed below. Theoretical affinities are in greater disaccord, with values ranging from 25.75 [20] to 54 meV [7]. At this level of precision, none of the experimental values considers the fine structure and all have to be interpreted as the barycentric value of  $^2D_{3/2}$  and  $^2D_{5/2}$ . The fine-structure splitting was computed to be as small as 0.22 meV ( $1.76 \text{ cm}^{-1}$ ) [20], and is not resolved in our experiment.

Table I presents the values of the binding energy  ${}^eA_{2D^o}$  obtained at different wavelengths. These values, with their experimental uncertainties, are deduced from a Bayesian analysis of the radial distribution with the help of Eqs. (7) to (9) and are combined in a weighted average to obtain, with a  $1\text{-}\sigma$  uncertainty, a first determination of the binding energy of the  $^2D^o$  state:

$${}^eA_{2D^o}^{\text{stat}} = 36.84(6) \text{ meV}. \quad (36)$$

Instead of considering a single wavelength at a time, we also explored an alternative approach, based this time on the global dependence of the radial position inside the VMI spectrometer on the energy of photodetached electrons. In an ideal spectrometer, we expect an exact verification of Eq. (6).

In Fig. 5, we plot the Bayesian estimation of the squared radius of the Newton spheres associated to channels (1) and (3) as a function of the photon energy. For the fine structure of the  $^4S^o$  state, we use the distribution given by Eq. (11), except for the two wavelengths under the threshold of channel (3) where the combination of amplitudes is left free. In that range, we expect some departure from Eq. (11) due to the Wigner threshold law affecting the rise of individual contributions in the vicinity of their respective thresholds. As the crossing point  $r_i = 0$  corresponds to the threshold  $E_i^{\text{th}}$  of channel  $i$ , we deduce

$$E_1^{\text{th}}(J=0) = 1262.085(34) \text{ meV}, \quad (37)$$

$$E_3^{\text{th}} = 1300.601(28) \text{ meV}. \quad (38)$$

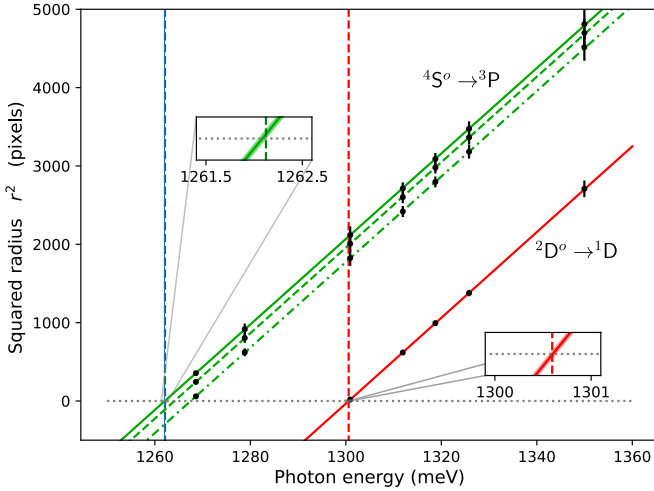


FIG. 5. Experimental squared radius as a function of photon energy (black filled circles). Green solid line, fit of channel  $4S^o \rightarrow 3P_0$ ; green dashed line, fit of channel  $4S^o \rightarrow 3P_1$ ; green dash-dotted line, fit of channel  $4S^o \rightarrow 3P_2$ ; red solid line, fit of channel  $2D^o \rightarrow 1D$ . The green vertical dashed line corresponds to the reference value [3] for  $4S^o \rightarrow 3P_0$  and the red vertical dashed line corresponds to our recommended value for  $2D^o \rightarrow 1D$ . The thickness of the solid lines corresponds to  $1\text{-}\sigma$  uncertainty of the fit.

The comparison of  $E_1^{\text{th}}(J=0)$  to the reference value from [3],

$${}^eA_{4S^o} = 1262.1226(11) \text{ meV}, \quad (39)$$

confirms the robustness of the approach. As a result, we obtain another estimate of the binding energy:

$${}^eA_{2D^o}^{\text{fit}} = E_3^{\text{th}} - E_{1D^o} = 36.87(3) \text{ meV}. \quad (40)$$

Considering the better performance in terms of precision of the second approach, we retain this final value for the binding energy of the excited state of  $C^-$ . Our result is in good agreement with the value published by Oparin *et al.* [23] but with a much improved accuracy.

### B. Asymmetry parameters and branching ratios

The asymmetry parameter  $\beta$  for channels (2) and (3) contributing to the photodetachment of  $2D^o$  is depicted in Fig. 6 as a function of photon energy. Their characteristic evolution with energy above threshold, i.e., a rapid decrease toward  $\beta = -1$  followed by a slow rise to positive values, results from the interference between  $s$ -wave and  $d$ -wave photodetachment of a bound  $p$  electron.

An extrapolation of individual  $\beta$  functions beyond the respective thresholds is also provided, in regions where experimental points were difficult to obtain as no light source was available or where the distinction between channels (1) and (3) was not possible within the resolution of our spectrometer. This extrapolation is based on the model of [26] for which the complete expression of the asymmetry parameter derived by Cooper and Zare [27] is simplified close to threshold, assuming a scaling law of the radial dipole element based on Wigner's threshold law. The asymmetry parameter is represented by a simple analytical formula with only two free

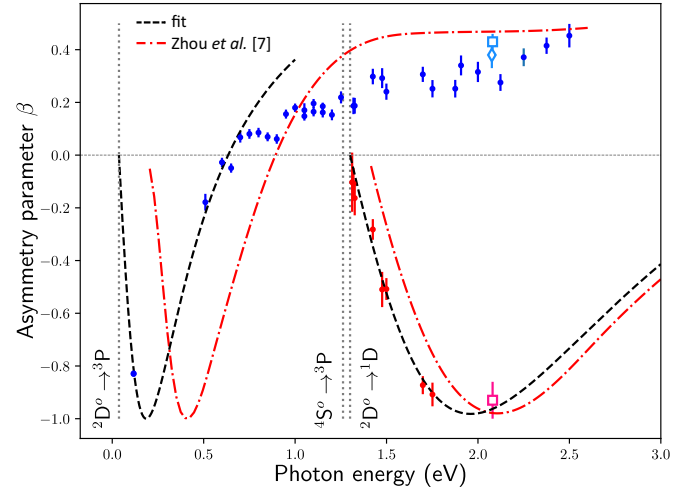


FIG. 6. Asymmetry parameter  $\beta$  as a function of photon energy. Blue symbols,  $2D^o \rightarrow 3P$ ; red symbols,  $2D^o \rightarrow 1D$ . Filled circles are experimental values from the present paper. Open symbols are experimental values from previous studies: the blue diamond is from [5]; blue and red squares are from [4]. Dashed lines are fits based on Eq. (41) from [26] in order to extrapolate the experimental points close to threshold. Red dash-dotted lines are the theoretical predictions from [7].

parameters  $\{A, c\}$ :

$$\beta = \frac{2A\varepsilon(A\varepsilon - 2c)}{1 + 2A^2\varepsilon^2} \quad (41)$$

where  $\varepsilon = E_{\text{ph}} - E^{\text{th}}$  is the kinetic energy of the detached electron, expressed in eV. Our best fit for channel (2) when enforcing  $\beta = 0$  at threshold is obtained with  $A_2 = 3.34 \text{ eV}^{-1}$ ,  $c_2 = 1$  and for channel (3) with  $A_3 = 0.75 \text{ eV}^{-1}$ ,  $c_3 = 0.99$ . Fitting functions are displayed over the range of experimental values actually included in the fit. No significant improvement of the fit could be gained by including all experimental points for channel (2), as expected from the limited range over which the Wigner threshold law is assumed to be valid. Evaluation of formula (19), with typically 25 000 recorded events of effective signal remaining after background subtraction, yields a precision of  $\Delta\beta \approx 0.05$ .

A comparison with the experimental points of [5] (blue diamond) and [4] (red and blue squares) shows a good agreement with our results while the theoretical predictions from [7] overestimate the energy at which the minimum of  $\beta$  is found. The global shape remains nevertheless in qualitative agreement with our results for negative values of  $\beta$  but starts to deviate significantly for positive values. While a simple shift seems to reconcile theory with experiment in the  $2D^o \rightarrow 1D$  case, some discrepancy persists for the  $2D^o \rightarrow 3P$  channel, as observed for the partial cross section (see below).

The branching ratio  $\Gamma_3$  defined by Eq. (21) for channels (2) and (3) is depicted in Fig. 7. Systematic uncertainties coming from background subtraction in VMI spectrometer images are far larger than statistical fluctuations and are estimated to  $\Delta\Gamma_3 = 0.03$ . The fitting function that we have used for extracting the partial cross sections over the relevant range depends on three parameters  $a, b$ , and  $c$  and is designed to tend to a Wigner law at threshold while becoming almost

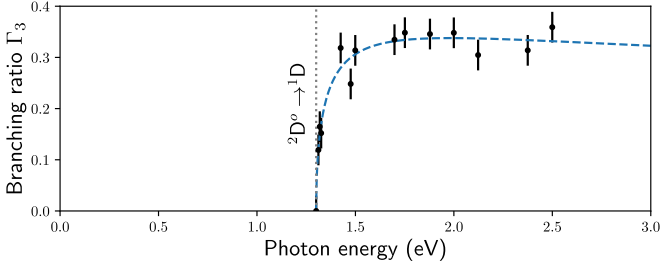


FIG. 7. Branching ratio  $\Gamma_3$  for channel  ${}^2D^0 \rightarrow {}^1D$  as a function of photon energy. Filled circles are experimental values extracted from the distribution of events recorded with the VMI spectrometer after Abel inversion. The dashed line is the fit function (42).

constant at higher energy:

$$\Gamma(\varepsilon) = a \frac{\sqrt{\varepsilon}}{1 + b\varepsilon^c}. \quad (42)$$

This formula was already proposed and successfully used in our study [11] of the absolute total, partial, and differential cross sections for photodetachment of  $O^-$ . Our best fit is obtained with  $a = 1.261 \text{ eV}^{-1/2}$ ,  $b = 2.766 \text{ eV}^{-0.74}$ , and  $c = 0.74$ . The relative uncertainty of the fit is dominated by systematic uncertainties on  $\Gamma_3$  and is conservatively fixed at 10%.

Finally, the state-specific contribution (22) is obtained by determining the  ${}^4S^0$  contribution in VMI images at a fixed wavelength but for decreasing laser pulse energies, and taking its zero pulse energy limit  $\gamma_{4S^0} = \lim_{E \rightarrow 0} \gamma(E)$ . Taking into account the precision of our method, estimated at 4% for  $\sigma^{\text{ACB}}$  [12], the final contributions for the different wavelengths and the deduced population are given in Table II. We determine from this analysis the population of the excited state in our beam:

$$p_{2D^0} = 29(3)\%. \quad (43)$$

In the high-energy limit, Serenkov *et al.* [8] predict a population of the electronic terms in proportion of their multiplicities, i.e.,  $p_{2D^0} : p_{4S^0} = 10 : 4$  for single-electron capture from alkali-metal targets. Such a large population of the excited state of  $C^-$  is to be contrasted with the minute

TABLE II. Experimental state-specific contribution  $\gamma_{4S^0}$ , ACB cross section (in units of  $10^{-22} \text{ cm}^2$ ),  ${}^4S^0$  cross section (in units of  $10^{-22} \text{ cm}^2$ ) [12], and corresponding population,  $p_{4S^0}$ .

$\lambda$ (nm)	$\gamma_{4S^0}$ (%)	$\sigma^{\text{ACB}}$	$\sigma_{4S^0}$	$p_{4S^0}$ (%)
870	55.4(1)	12.5(5)	16.3(7)	73(4)
840	56.2(3)	13.0(6)	17.0(7)	73(4)
730	54.4(2)	14.5(6)	17.5(7)	68(4)
Average				71(3)

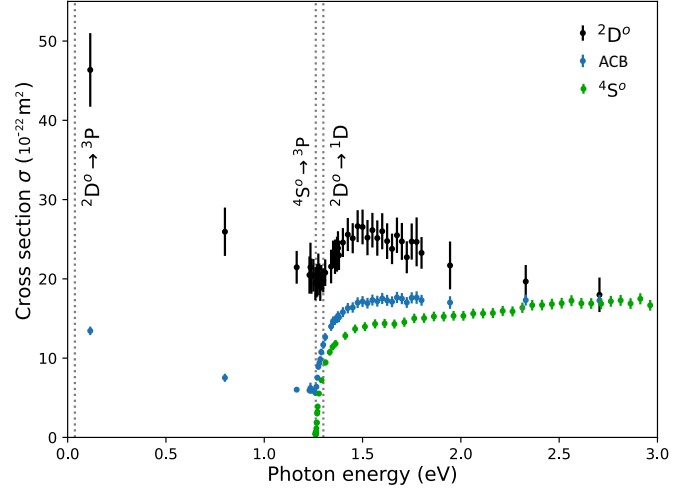


FIG. 8. Experimental results of ACB measurements with cw laser. Blue filled circles are the present cross section measured for the mixture of ground and excited states. Based on the population (43) and the photodetachment cross section of  $C^-({}^4S^0)$  from [12] represented by the green filled circles, the total photodetachment cross section of  $C^-({}^2D^0)$  is given by the black filled circles. Error bars represent 1- $\sigma$  uncertainty.

population observed with gas discharge and cesium sputtering ion sources.

### C. Cross sections

The only previous measurement of the photodetachment cross section of  $C({}^2D^0)$  was performed at  $E_{\text{ph}} = 2.076 \text{ eV}$  [4] and produced the following partial cross sections  $\sigma_i$ :

$$\sigma_2 \equiv \sigma_{2D^0 \rightarrow 3P} = 13(2) \times 10^{-22} \text{ m}^2,$$

$$\sigma_3 \equiv \sigma_{2D^0 \rightarrow 1D} = 5(2) \times 10^{-22} \text{ m}^2,$$

which add up to a total cross section

$$\sigma_{2D} \equiv \sigma_2 + \sigma_3 = 18(3) \times 10^{-22} \text{ m}^2.$$

This absolute value was calibrated against  $D^-$  photodetachment.

The present results obtained for the absolute photodetachment cross section of a mixture of  ${}^4S^0$  and  ${}^2D^0$  states are presented in Fig. 8, with only the points obtained using cw lasers for clarity. Applying formula (33) to these values with the help of the population (43) determined above and the cross section obtained independently in [12] for the ground state, the total cross section for the excited state  $\sigma_{2D^0}$  may finally be obtained and is also plotted in Fig. 8.

The precision on these values can be estimated by computing the variance (var) of expression (33), assuming that all variables involved are independent and that the relative precision on the presently measured  $\sigma^{\text{ACB}}$  and the previously published  $\sigma_{4S^0}$  is of 4%:

$$\begin{aligned} \text{var}[\sigma_{2D^0}] \equiv & \frac{1}{(1 - p_{4S^0})^2} \text{var}[\sigma^{\text{ACB}}] + \frac{p_{4S^0}^2}{(1 - p_{4S^0})^2} \text{var}[\sigma_{4S^0}] \\ & + \left( \frac{\sigma^{\text{ACB}} - \sigma_{4S^0}}{(1 - p_{4S^0})^2} \right)^2 \text{var}[p_{4S^0}]. \end{aligned} \quad (44)$$

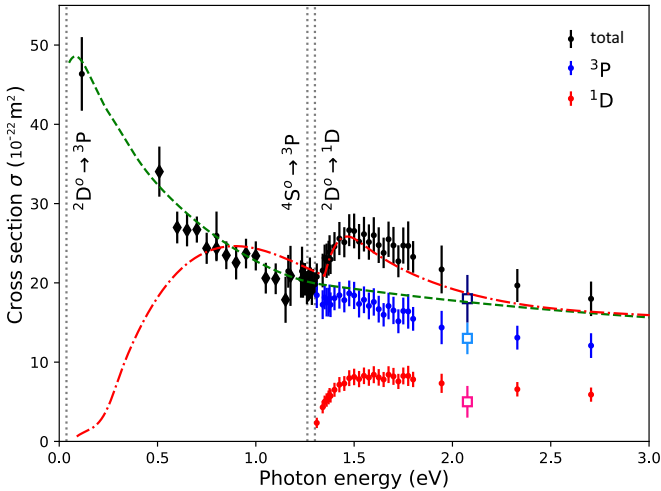


FIG. 9. Absolute total and partial photodetachment cross sections for  $C^-(^2D^0)$  as a function of photon energy. The black filled circles are the experimental values obtained with cw laser and the black diamonds with pulsed laser. The blue filled circles are the partial cross section for  $^2D^0 \rightarrow ^3P$ , and red filled circles for  $^2D^0 \rightarrow ^1D$ . Open squares are the experimental values from [4] and their sum. The green dashed line is the prediction of Ramsbottom *et al.* [6] and the red dash-dotted line is the prediction of Zhou *et al.* [7].

With typical values of  $\sigma_{2D^0} = 26 \times 10^{-22} \text{m}^2$ ,  $\sigma^{\text{ACB}} = 17 \times 10^{-22} \text{m}^2$ ,  $\sigma_{4S^0} = 14 \times 10^{-22} \text{m}^2$ , and  $p_{4S^0} = 0.71$ , the relative uncertainty reaches  $\Delta\sigma_{2D^0}/\sigma_{2D^0} \approx 12\%$ .

The use of the branching ratio defined by Eq. (42) allows the determination of partial cross sections and their comparison to other experimental and theoretical results. The final result obtained in this paper as well as the previous experimental results [4] and theoretical predictions [6,7] are shown in Fig. 9.

The experimental points of Brandon *et al.* [4] obtained for partial and total cross sections agree with ours within error bars.

We observe that none of the theoretical models is valid over the entire investigated range. Nevertheless, we can distinguish the range from the  $^3P$  to the  $^1D$  threshold where the calculations of Ramsbottom *et al.* [6] are in excellent agreement with our results, and energies above the  $^1D$  threshold where these calculations fail to account for the importance of this additional channel. In contrast, the results of Zhou *et al.* [7] behave much more satisfactorily above the  $^1D$  threshold, although this threshold is slightly too high in the calculations. On the other hand, the latter calculations entirely miss the rapid onset of the cross section at the opening of the  $^2D^0 \rightarrow ^3P$  threshold. In view of the claim by Zhou *et al.* that their calculation is actually converged by comparison of the length and velocity gauge results, one is left with a real theoretical puzzle.

#### IV. CONCLUSIONS

We have reported here the results obtained for the photodetachment of the  $^2D^0$  excited state of  $C^-$ . Using the method of charge exchange with a vapor of Cs, we have succeeded in producing a mixed beam with 29% of the population in the  $^2D^0$  excited state and the rest in the  $^4S^0$  ground state.

With an improved data analysis of the radial distribution of events recorded with a VMI spectrometer, we propose updating the benchmark value for the binding energy of the excited state to  $^4A_{2D^0} = 36.87(3)$  meV, in agreement with the value obtained by Oparin *et al.* [23].

Using the ACB and VMI techniques complemented with an adapted data processing in order to deal with a beam composed of a mixture of ground and excited states, we have significantly extended the ensemble of available experimental values for the absolute total and partial cross sections, now with photon energies ranging from near threshold (0.12 eV) to 2.7 eV, thus providing a benchmark for existing and future theoretical work. The lowest channel,  $^2D^0 \rightarrow ^3P$ , is well reproduced by the calculations of Ramsbottom *et al.* [6] while the next channel,  $^2D^0 \rightarrow ^1D$ , is better described by the more recent calculations of Zhou *et al.* [7]. The absolute cross sections are in good agreement with the values published by Brandon *et al.* [4] for  $E_{\text{ph}} = 2.076$  eV.

An important result of this paper concerns the magnitude of the cross section in the vicinity of the  $^2D^0 \rightarrow ^3P$  threshold, which enters the determination of the  $C^-(^2D^0)$  lifetime in a blackbody radiation field. Experimental observations at the Tokyo Metropolitan University electrostatic ion storage ring [28] have determined a lifetime of 2.7 ms at room temperature. Would the cross section have followed the prediction of Zhou *et al.* [7], the blackbody photodetachment would have been insignificant, contradicting observations made at the storage ring.

We have also measured the asymmetry parameter in the same energy range, and compared our results with those of Zhou *et al.* The latter qualitatively reproduce our measurements. The present values for the  $^2D^0 \rightarrow ^3P$  and  $^2D^0 \rightarrow ^1D$  channels are in good agreement with the only experimental points ( $E_{\text{ph}} = 2.076$  eV) existing in the literature [4,5].

The disagreement between available theoretical data, and their disaccord with our experimental results, show that the excited state of  $C^-$ , a system in which the delicate balance between attraction by a polarized atomic core and electronic repulsion is responsible for a very small binding energy of 36.87(3) meV, remains a formidable challenge for future theoretical work. Our paper provides benchmark data that can be used to assess these methods over a broad range of energies and for a complete set of cross sections.

The unique combination of electron spectrometry and animated beam cross-section measurements is a promising avenue to tackle more complex anions. One obvious candidate is  $\text{Si}^-$ , having no less than four excited levels with lifetimes ranging between tens of seconds and hours [29]. Small molecular anions such as  $\text{OH}^-$  are natural targets for a similar study. State-selective photodetachment of  $\text{OH}^-$  has been applied as a thermometer to probe radiative cooling in cryogenic ion storage devices [30–32], while the knowledge of its rovibrationally resolved photodetachment cross section remains fragmentary [33–35].

#### ACKNOWLEDGMENTS

The authors thank M. Génévriez, M. Terao-Dunseath, and K. M. Dunseath for useful discussions and their critical



reading of the paper. This work was supported by the Fonds de la Recherche Scientifique - FNRS through Grant No.

4.4504.10. X.U. is a Senior Research Associate of the Fonds de la Recherche Scientifique - FNRS.

- 
- [1] T. Andersen, *Phys. Rep.* **394**, 157 (2004).
- [2] M. Scheer, R. C. Bilodeau, C. A. Brodie, and H. K. Haugen, *Phys. Rev. A* **58**, 2844 (1998).
- [3] D. Bresteau, C. Drag, and C. Blondel, *Phys. Rev. A* **93**, 013414 (2016).
- [4] W. D. Brandon, D. H. Lee, D. Hanstorp, and D. J. Pegg, *J. Phys. B* **31**, 751 (1998).
- [5] D. J. Pegg, C. Y. Tang, J. Dellwo, and G. D. Alton, *J. Phys. B* **26**, L789 (1993).
- [6] C. A. Ramsbottom, K. L. Bell, and K. A. Berrington, *J. Phys. B* **26**, 4399 (1993).
- [7] H.-L. Zhou, S. T. Manson, A. Hibbert, L. Vo Ky, and N. Feautrier, *Phys. Rev. A* **72**, 032723 (2005).
- [8] I. Serenkov, R. Il'in, V. Oparin, and E. Solov'ev, *Zh. Eksp. Teor. Fiz.* **68**, 1686 (1975) [*Sov. Phys. JETP* **41**, 845 (1975)].
- [9] X. Urbain, D. Bech, J.-P. Van Roy, M. Géléoc, S. J. Weber, A. Huetz, and Y. J. Picard, *Rev. Sci. Instrum.* **86**, 023305 (2015).
- [10] M. Génévriez and X. Urbain, *Phys. Rev. A* **91**, 033403 (2015).
- [11] M. Génévriez, K. M. Dunseath, M. Terao-Dunseath, A. Hibbert, A. Dochain, R. Marion, and X. Urbain, *Phys. Rev. A* **98**, 033410 (2018).
- [12] R. Marion, K. M. Dunseath, M. Terao-Dunseath, and X. Urbain, *Phys. Rev. A* **103**, 023115 (2021).
- [13] R. Marion, M. Čížek, and X. Urbain, *Phys. Rev. A* **107**, 052808 (2023).
- [14] P. C. Engelking and W. C. Lineberger, *Phys. Rev. A* **19**, 149 (1979).
- [15] C. Blondel, W. Chaibi, C. Delsart, and C. Drag, *J. Phys. B* **39**, 1409 (2006).
- [16] C. Pan and A. F. Starace, *Phys. Rev. A* **47**, 295 (1993).
- [17] O. Scharf and M. R. Godefroid, [arXiv:0808.3529](https://arxiv.org/abs/0808.3529).
- [18] DLMF, NIST Digital Library of Mathematical Functions, edited by F. W. J. Olver, A. B. Olde Daalhuis, D. W. Lozier, B. I. Schneider, R. F. Boisvert, C. W. Clark, B. R. Miller, B. V. Saunders, H. S. Cohl, and M. A. McClain, <https://dlmf.nist.gov/>, release 1.1.11 (15 Sept. 2023).
- [19] S. J. Cavanagh, S. T. Gibson, M. N. Gale, C. J. Dedman, E. H. Roberts, and B. R. Lewis, *Phys. Rev. A* **76**, 052708 (2007).
- [20] T. Carette and M. R. Godefroid, *Phys. Rev. A* **83**, 062505 (2011).
- [21] K. Haris, A. Kramida, and NIST ASD Team, Critically Evaluated Spectral Data for Neutral Carbon (CI), NIST Atomic Spectra Database (ver. 5.10), <https://physics.nist.gov/asd> (2017).
- [22] B. Dick, *Phys. Chem. Chem. Phys.* **16**, 570 (2014).
- [23] V. Oparin, R. N. Il'in, I. T. Serenkov, and E. S. Solov'ev, *Zh. Eksp. Teor. Fiz.* **66**, 2008 (1974) [*Sov. Phys. JETP* **39**, 989 (1974)].
- [24] D. Feldmann, *Chem. Phys. Lett.* **47**, 338 (1977).
- [25] T. Andersen, H. K. Haugen, and H. Hotop, *J. Phys. Chem. Ref. Data* **28**, 1511 (1999).
- [26] D. Hanstorp, C. Bengtsson, and D. J. Larson, *Phys. Rev. A* **40**, 670 (1989).
- [27] J. Cooper and R. N. Zare, *J. Chem. Phys.* **48**, 942 (1968).
- [28] T. Takao, S. Jinno, K. Hanada, M. Goto, K. Oshikiri, K. Okuno, H. Tanuma, T. Azuma, and H. Shiromaru, *J. Phys.: Conf. Ser.* **88**, 012044 (2007).
- [29] D. Müll, F. Grussie, K. Blaum, S. George, J. Göck, M. Grieser, R. von Hahn, Z. Harman, A. Kálosi, C. H. Keitel, C. Krantz, C. Lyu, O. Novotný, F. Nuesslein, D. Paul, V. C. Schmidt, S. Singh, S. Sunil Kumar, X. Urbain, A. Wolf, and H. Kreckel, *Phys. Rev. A* **104**, 032811 (2021).
- [30] F. Goldfarb, C. Drag, W. Chaibi, S. Kröger, C. Blondel, and C. Delsart, *J. Chem. Phys.* **122**, 014308 (2005).
- [31] C. Meyer, A. Becker, K. Blaum, C. Breitenfeldt, S. George, J. Göck, M. Grieser, F. Grussie, E. A. Guerin, R. von Hahn, P. Herwig, C. Krantz, H. Kreckel, J. Lion, S. Lohmann, P. M. Mishra, O. Novotný, A. P. O'Connor, R. Repnow, S. Saurabh, D. Schwalm, L. Schweikhard, K. Spruck, S. Sunil Kumar, S. Vogel, and A. Wolf, *Phys. Rev. Lett.* **119**, 023202 (2017).
- [32] H. T. Schmidt, G. Eklund, K. C. Chartkunchand, E. K. Anderson, M. Kamińska, N. de Ruelle, R. D. Thomas, M. K. Kristiansson, M. Gatchell, P. Reinhard, S. Rosén, A. Simonsson, A. Källberg, P. Löfgren, S. Mannervik, H. Zettergren, and H. Cederquist, *Phys. Rev. Lett.* **119**, 073001 (2017).
- [33] L. M. Branscomb, *Phys. Rev.* **148**, 11 (1966).
- [34] L. C. Lee and G. P. Smith, *J. Chem. Phys.* **70**, 1727 (1979).
- [35] P. Hlavenka, R. Otto, S. Trippel, J. Mikosch, M. Weidemüller, and R. Wester, *J. Chem. Phys.* **130**, 061105 (2009).